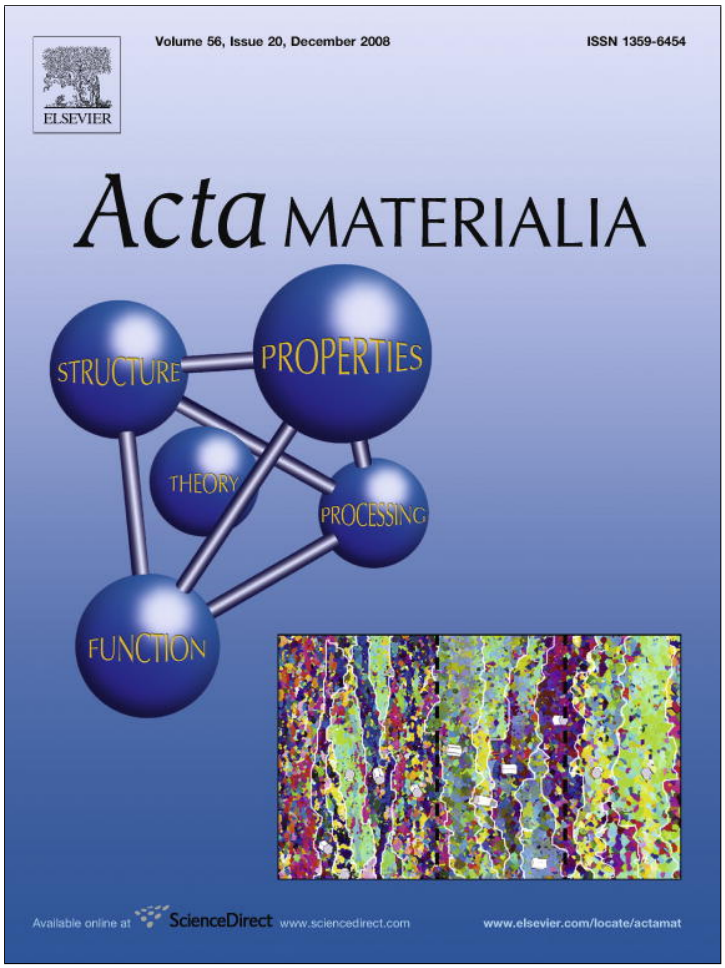

Available online at www.sciencedirect.com
ScienceDirect
Acta Materialia 56 (2008) 6246–6256
Acta MATERIALIA
www.elsevier.com/locate/actamat

Increase of Co solubility with decreasing grain size in ZnO

B.B. Straumal [a,b,c,*], A.A. Mazilkin [b], S.G. Protasova [b], A.A. Myatiev [c], P.B. Straumal [c,d], B. Baretzky [a]

[a] Max-Planck-Institut für Metallforschung, Heisenbergstrasse 3, 70569 Stuttgart, Germany
[b] Institute of Solid State Physics, Russian Academy of Sciences, Chernogolovka, Moscow District 142432, Russia
[c] Moscow Institute of Steel and Alloys (Technological University), Leninsky Prospect 4, 119991 Moscow, Russia
[d] Institut für Materialphysik, Universität Münster, Wilhelm-Klemm-Str. 10, D-48149 Münster, Germany

Received 6 April 2008; received in revised form 11 August 2008; accepted 20 August 2008
Available online 22 September 2008

Abstract

Nanograined (grain size 10 nm) ZnO films with various Co contents (0–52 at.% Co) were synthesized by a novel liquid ceramics method. The solubility limit for Co was determined at 550 °C. The lattice parameter c of the ZnO-based solid solution with würzite structure ceases to grow at 33 at.% Co. The peaks of the second phase (Co_2O_3 or with cubic lattice) become visible in the X-ray diffraction spectra at 40 at.% Co. The same second phase appears in the bulk ZnO already at 2 at.% Co [Bates CH, White WB, Roy R. J Inorg Nucl Chem 1966;28:397]. A few years ago it was predicted theoretically that ZnO could become ferromagnetic at room temperature and above by doping with Co and other transition metals. Recently published papers on the structure and magnetic behaviour of Co-doped ZnO allowed us to obtain the size dependence of Co solubility in ZnO for the polycrystals and small single-crystalline particles. The overall Co solubility drastically increases with decreasing grain size. The quantitative estimation leads to the conclusion that, close to the bulk solubility limit, the thickness of a Co-enriched layer is several monolayers in grain boundaries and at least two monolayers in the free surfaces.

Keywords: Grain boundaries; Surfaces; Solubility; Phase diagrams; Zinc oxide

1. Introduction

In two-component and multicomponent alloys, by increasing the content of an alloying component, c, a solubility limit is reached at a certain concentration, c_s. Above c_s, the second phase appears in the bulk. By further increasing c, only the amount of the second phase increases, but the concentration in the first phase remains equal to c_s. The volume solubility limit c_s increases with increasing temperature. The easiest way to measure c_s is to follow the change of the lattice spacing in the solid solution, for example with the help of X-ray diffraction (XRD). The lattice spacing continuously changes (it can either increase or decrease) with increasing c up to c_s. At $c > c_s$ the lattice spacing remains unchanged, and the diffraction peaks of the second phase appear in the XRD spectrum.

If the alloy contains surfaces and interfaces enriched by a second component, the total concentration of this second component, c_t, will be higher than its concentration in the bulk solid solution, c_v. The difference between c_t and c_v increases with an increasing specific area of surfaces and interfaces (i.e., with decreasing grain size). If the grain size is small enough, the difference between c_t and c_v can become measurable. This is due to the fact that XRD registers the diffraction only from the bulk phases. The component located in the thin surface or interface layers remains invisible for XRD. The XRD peaks appear only in the case when the coherent-scattering region is large enough (grain size around 5 nm or larger). At the same

* Corresponding author. Address: Max-Planck-Institut für Metallforschung, Heisenbergstrasse 3, 70569 Stuttgart, Germany. Tel.: +7 9166768673; fax: +7 4992382326.
E-mail address: straumal@issp.ac.ru (B.B. Straumal).

1359-6454/$34.00 © 2008 Acta Materialia Inc. Published by Elsevier Ltd. All rights reserved.
doi:10.1016/j.actamat.2008.08.032

time, XRD allows one to measure the grain size using the angle dependence of the peak width.

McLean proposed that the apparent solubility limit, c_{sa}, in fine-grained materials will be higher than the volume solubility limit c_s [1]. He calculated this difference for the Fe–C system with grain sizes of 1 and 10 μm for the case of simple Langmuir-like grain boundary segregation [1]. There are many indications in the literature that $c_{sa} > c_s$ in micro- and nanograined materials [2–7]. However, the consistent XRD measurements of solubility shift c_{sa}–c_s with grain size d are very time consuming and, to the best of our knowledge, have never been conducted before. ZnO offers a good possibility for such an investigation. ZnO is widely used as a transparent conducting oxide in the semiconductor thin film technology, as a material for varistors (doped with Bi_2O_3) and for gas sensors. Moreover, it is a promising material for future spintronics as a possible ferromagnetic semiconductor. Ferromagnetic semiconductors could allow seamless electrical manipulations of magnetic states and magnetic modification of electric signals. In 2000 Dietl et al. predicted theoretically that ZnO doped by small amounts of "magnetic" impurities such as Mn or Co would possess ferromagnetic properties [8]. This work triggered a boom in experimental work, and more than 1200 papers devoted to dilute magnetic semiconductors have since been published. Unfortunately, ferromagnetism in diluted doped ZnO is far from understood. The presence or absence of ferromagnetism in doped ZnO critically depends on the synthesis method. However, these studies allow the dependence of c_{sa}–c_s on the grain (particle) size d to be calculated.

Therefore, the goal of this work is threefold: (i) to measure the solubility shift c_{sa}–c_s in nanograined ZnO manufactured by a novel liquid ceramics method; (ii) to analyze the c_{sa}–c_s dependence on the grain size over a broad interval of d using the published data on ZnO; (iii) to compare the influence of Co-enrichment in surfaces and interfaces (i.e., grain boundaries, GBs) on the shift c_{sa}–c_s at the same grain (particle) size d.

2. Materials and methods

The Co-doped ZnO thin films were deposited on the Al foils by a novel liquid ceramics method. The substrates were dip-coated with a mixture of liquid organic acids and metallic ions, and dried at 150 °C. The deposited layers were then oxidized in air at 550 °C. The resulting films were greenish and transparent. The film thickness was determined by the electron-probe microanalysis (EPMA) and edge-on transmission electron microscopy (TEM) and measured between 50 and 200 nm. The Co content in films was between 0 and 52 at.%. The Zn and Co content in doped oxides was measured by atomic absorption spectroscopy in a Perkin-Elmer spectrometer and by EPMA in a Tescan Vega TS5130 MM microscope equipped with an Oxford Instruments LINK energy-dispersive spectrometer. TEM investigations were carried out on a JEM-4000FX microscope at an accelerating voltage of 400 kV. TEM was used to investigate the crystal structure of the film, especially at the interface, and to look for possible Co clusters. TEM was also used to measure the grain size in pure and doped ZnO films. XRD data were obtained on a Siemens diffractometer (with Fe Kα radiation) with a graphite monochromator and line-position-sensitive gas flow detector. Calculation of the grain size, d, was done using the angle dependence of the peak broadening [9]. The grain size in all studied samples was 10 ± 2 nm.

3. Results and discussion

Fig. 1a shows a bright-field high-resolution electron micrograph of the nanograined ZnO thin film. The electron diffraction pattern is shown in Fig. 1b. The deposited ZnO film is dense, non-porous, nanograined, uniform and non-textured. The grain size in this film is about 10 nm. In Fig. 2 two XRD spectra are shown: for pure ZnO (bottom) and ZnO doped with 40 at.% Co. Only würzite lines are visible in the pure ZnO film. The cubic Co_2O_3 phase appears additionally in the ZnO–40 at.% Co sample. In Fig. 3 the dependence of the lattice parameter c in the Co-doped ZnO films on the Co concentration is shown. The error bars in Fig. 2 are defined by the angular error for the peak positions in XRD spectra. The lattice spacing linearly increases up to 33 at.% Co. Above 33 at.% Co, the second phase Co_2O_3 with cubic structure appears and the lattice spacing in the würzite ZnO phase ceases to increase. This

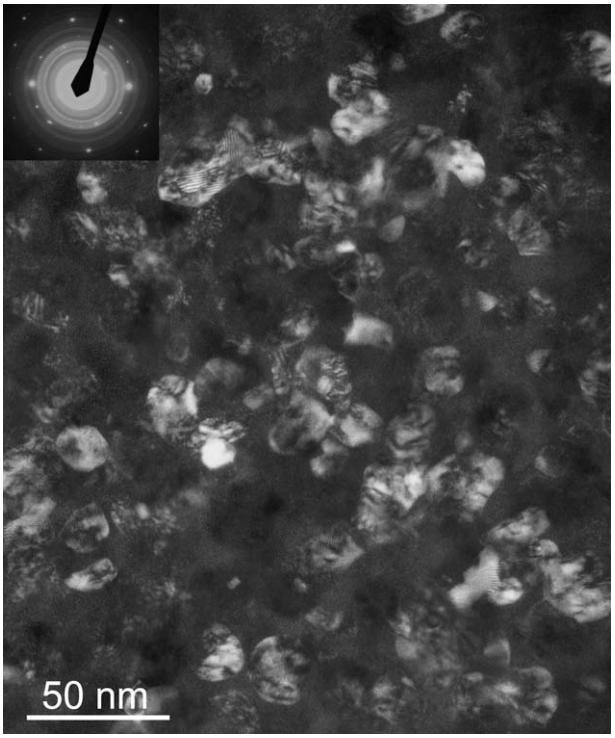

Fig. 1. Dark-field TEM micrograph of the nanograined ZnO thin film deposited by the liquid ceramics technology, with the electron diffraction pattern as an insert. No texture is visible. Reflexions from the Al substrate are also present.

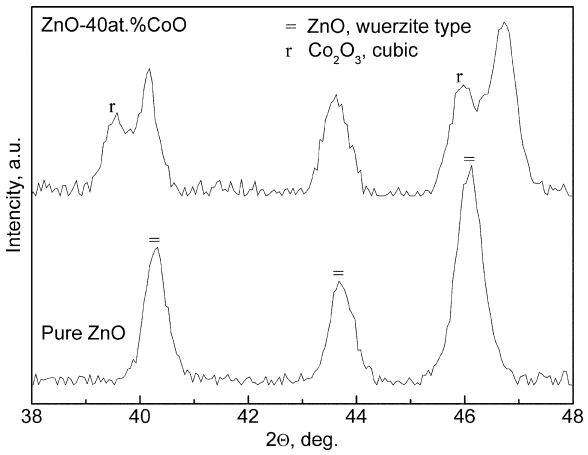

Fig. 2. XRD spectra for pure ZnO (bottom) and ZnO doped by 40 at.% CoO. Only würzite lines are visible in the pure ZnO film. The cubic Co_2O_3 phase appears additionally in the ZnO–40 at.% CoO sample.

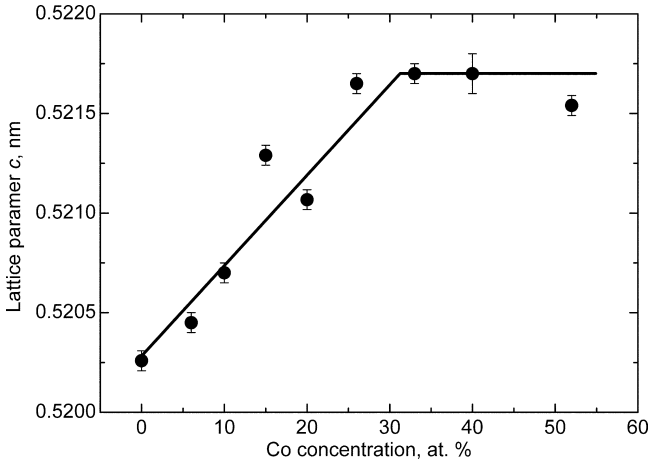

Fig. 3. Dependence of lattice parameter c in Co-doped ZnO films on the Co concentration.

means that the solubility limit c_{sa} in the Co-doped ZnO thin films with a grain size 10 nm is 33 at.% Co at 550 °C. The solubility limit in the bulk c_s is about 2 at.% Co at 550 °C [10].

In order to find ferromagnetism in doped ZnO, it is important to ensure that it does not contain any particles from the second phase which could influence the sample's magnetic properties. This means that in each published work the data on the dopant concentration are presented, and presence or absence of a second phase is noted. Usually, the presence or absence of a second phase is controlled by XRD. Measurable X-ray peaks appear in the diffraction spectra when the amount of a second phase is about 1–2%. TEM or Raman spectroscopy allows one to detect a second phase at lower content than XRD. However, such data are almost absent in the papers devoted to the magnetic behaviour of ZnO. Therefore, we used only XRD data for the construction of plots presented in Figs. 4–8. The majority of published works allowed us to estimate the grain or particle size and to assign the data to a certain temperature,

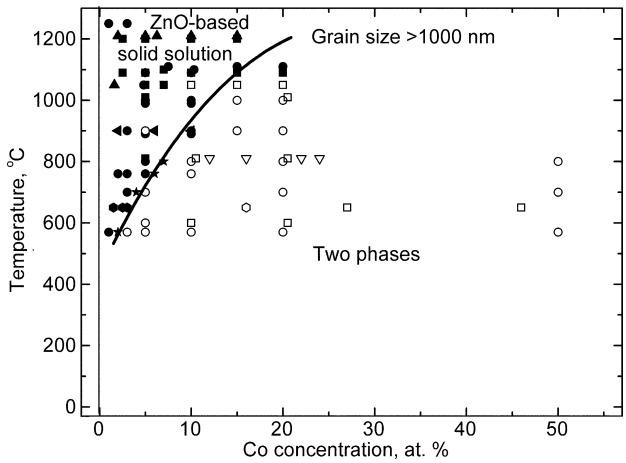

Fig. 4. Solubility limit of Co in ZnO polycrystals with grain sizes above 1000 nm [10–28]. Solid symbols correspond to the single-phase samples. Open symbols correspond to the two-phase samples. Filled stars correspond to the solubility limit. Rings correspond to the samples obtained by hydrothermal growth, growth from the melt, high-temperature and high-pressure synthesis of bulk crystals, and Co diffusion from the vapour into ZnO single crystals [10–13]; down-triangles, Co ion implantation into ZnO single-crystalline substrate [14]; up-triangles, chemical vapour transport [15,16]; squares, sintering of conventional powders [17–24]; left-triangles, co-precipitation [25]; hexagons, dual-beam pulsed laser deposition [26–28].

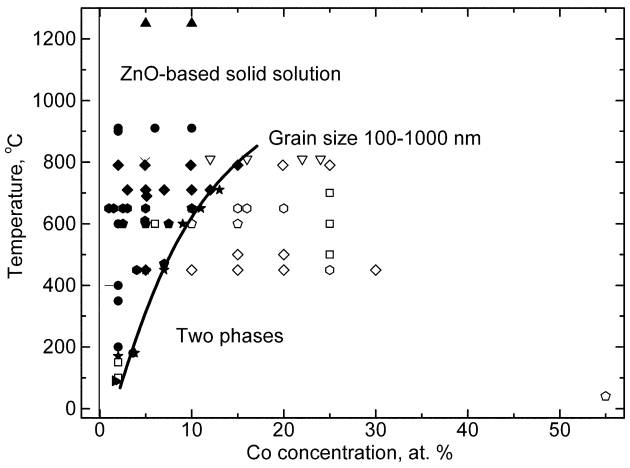

Fig. 5. Solubility limit of Co in ZnO polycrystals with grain sizes between 100 and 1000 nm [14,26–47] Solid symbols correspond to the single-phase samples. Open symbols correspond to the two-phase samples. Filled stars correspond to the solubility limit. Squares correspond to the samples obtained by the sintering of fine powders [29–32]; up-triangles, vapourization–condensation method [33]; pentagons, magnetron sputtering [34–37]; diamonds, sol–gel method [37–41]; right-triangles, electrodeposition [42,43]; down-triangles, Co ion implantation into ZnO single-crystalline substrate [14]; hexagons, single and DBPLD [26–28,44–47].

either that of a synthesis or of a final thermal treatment. The published data encompass grain (particle) sizes d from 10 mm to 10 nm and temperatures from 300 to 1500 K. This gave us the unique chance to construct the $c_{sa}(T)$ dependences for a broad interval of d and to compare the influence of internal boundaries and surfaces. The biggest data arrays exist for Co- and Mn-doped ZnO. In this work we will analyze the Co-doped ZnO.

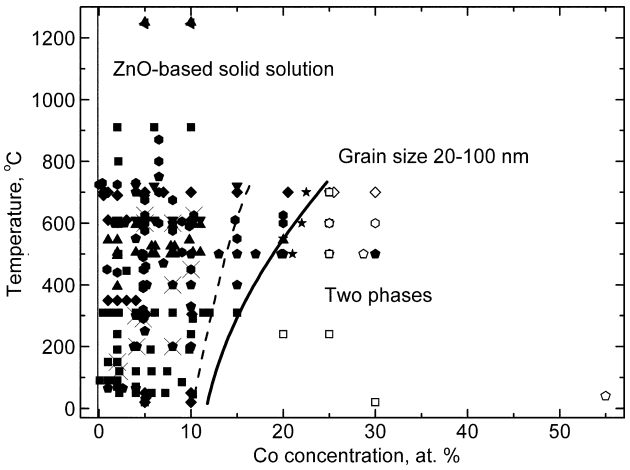

Fig. 6. Solubility limit of Co in ZnO polycrystals with grain sizes between 20 and 100 nm [29,36,37,48,30,49–109]. Solid symbols correspond to the single-phase samples. Open symbols correspond to the two-phase samples. Filled stars correspond to the solubility limit. Squares correspond to the samples obtained by the full or partial sintering of the very fine powders and partial sintering of nanowires [29,48,30,49–65]; left-triangles, auto-combustion method [66]; up-triangles, vapourization–condensation method [33]; pentagons, magnetron sputtering [36,37,67–76] and ion beam sputtering [77]; down-triangles, ion implantation [78–80]; diamonds, sol–gel method [84–90]; left-triangles, chemical vapour deposition [91–93]; hexagons, pulsed laser deposition [46,94–109] and molecular beam epitaxy [81–83]. Crosses correspond to the experiments where TEM investigations were performed; GBs are visible in TEM micrographs and GB Co-rich phases are absent [29,46,70,73–75,83,94–96,103].

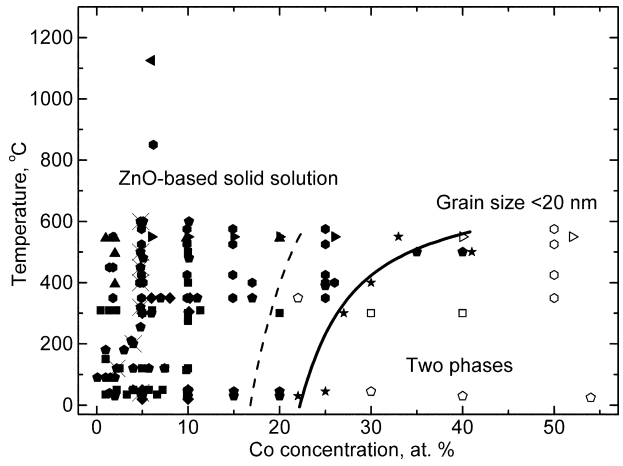

Fig. 7. Solubility limit of Co in ZnO polycrystals with grain sizes below 20 nm [26–28,35,49,60,62,68,71,73,74,76,85,86,91,92,97,105,110–126]. Solid symbols correspond to the single-phase samples. Open symbols correspond to the two-phase samples. Filled stars correspond to the solubility limit. Squares correspond to the samples obtained by the sintering of the very fine powders and partial sintering of nanowires [49,60,62,97,110–112,114]; left-triangles, solution combustion method [113]; pentagons, magnetron sputtering [35,68,71,73,74,76,115–121] and ion beam sputtering [122,123]; diamonds, sol–gel method [85,86]; up-triangles, chemical vapour deposition [91,92]; hexagons, pulsed laser deposition [26–28,105,124–126]; right-triangles, liquid ceramics method. Crosses correspond to the experiments where TEM investigations were performed; GBs are visible in TEM micrographs and GB Co-rich phases are absent [105,117,120,123].

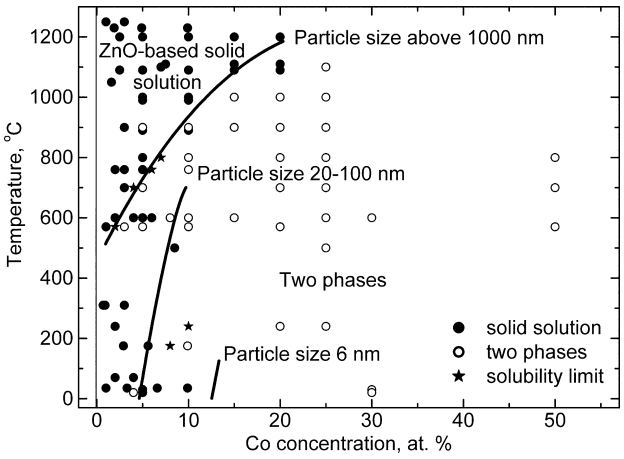

Fig. 8. Solubility limit of Co in ZnO powders with various particle sizes [10–12,15–18,32,19,127–132]. Solid symbols correspond to the single-phase samples. Open symbols correspond to the two-phase samples. Filled stars correspond to the solubility limit.

In Fig. 4 the solubility limit (solvus) of Co in ZnO polycrystals is drawn using the data on polycrystals with a grain size above 1000 nm [10–28]. (The errors in Fig. 4, as well as in Figs. 5–8 are below the scale of the markers.) These samples were obtained by hydrothermal growth [10], growth of Co-doped ZnO single crystals from the melt [11], high-temperature and high-pressure synthesis of bulk crystals [12], Co diffusion from the vapour into ZnO single crystals [13], Co ion implantation into ZnO single-crystalline substrate [14], chemical vapour transport [15,16], sintering of conventional powders [17–24], co-precipitation [25], and dual-beam pulsed laser deposition (PLD) [26–28]. Full symbols correspond to the single-phase samples. Open symbols correspond to the samples where the second phase Co_2O_3 was observed by XRD. Stars correspond to the solubility limit determined in the literature by the method similar to that used by us in Fig. 3. The experimental error of the synthesis or annealing temperature is usually below ±10 °C and the error of determination of Co concentration in ZnO is usually below ±0.1 at.%. Therefore, the error bars are not visible on the scale of the Figs. 4–8. The solubility of Co in ZnO reaches about 20 at.% at 1200 °C and falls below 2 at.% at 550 °C. This line corresponds to the solubility in the bulk of ZnO; the number of Co atoms segregated in grain boundaries is negligible.

Using the hydrothermal technique the oxide mixtures of known compositions were sealed together with a small amount of NaOH in water as a mineralizer in gold tubes and heated in a hydrothermal pressure vessel at 10^8 Pa and temperatures between 570 and 800 °C [10]. The grain size of doped ZnO was above 5 μm. High-temperature (900–1100 °C) and high-pressure (6 GPa) annealing of the original $ZnO + Co + Co_3O_4$ mixture in the sealed gold capsule without any mineralizer allowed large Co-doped ZnO bulk polycrystals to be manufactured [12]. In the vapour-phase diffusion method Co atoms were introduced into the few large (of the order of millimeters) ZnO single

crystals in a conventional tube furnace in flowing O_2 gas at 1050 °C for about 100 h. Co_3O_4 vapour was used as the source material which was evaporated from Co_3O_4 powder (melting point ~900 °C) [13]. In the ion-implantation method the commercial ZnO single-crystal substrates (0.5 mm thick) were implanted with Co with an energy of 100 keV and a fluence up to 10^{17} ions cm^{-2} [14]. The chemical vapour transport method allows some millimeter-scale Co-doped bulk ZnO single crystals to be manufactured [15,16]. By sintering of conventional powders, the ZnO and CoO powders with grain size between 1 and 20 μm were mixed together, pressed into pellets and annealed at temperatures between 600 and 1400 °C [17–24]. In the co-precipitation technique, the $Zn_{1-x}Co_xO$ powders were prepared by the decomposition of an oxalate precursor in which Co and Zn ions are already mixed [25]. The resulting powders with sizes above 1 μm were annealed at 900 °C [25]. In the dual-beam pulsed laser deposition (DBPLD), the laser beam was split into two beams and irradiated two separate targets of ZnO and Co. The two targets were ablated separately, and the Co-doped ZnO is thus formed by the growth of thin film on the single-crystal sapphire substrate from the fluxes coming from the two targets. The substrate temperature was between 600 and 800 °C. Usually DBPLD leads to the formation of rather fine-grained polycrystals; however, the grain size can be above 1000 nm with high Co concentrations [26–28].

In Fig. 5 the solubility limit (solvus) of Co in ZnO polycrystals is drawn using the data on polycrystals with grain size between 100 and 1000 nm [14,26–47]. These samples were obtained by sintering fine powders [29–32], vapourization–condensation method [33], magnetron sputtering [34–37], sol–gel method [37–41], electrodeposition [42,43], Co ion implantation into ZnO single-crystalline substrate [14], single- and dual-beam PLD [26–28,44–47]. The solubility of Co in ZnO reaches about 16 at.% at 800 °C and falls below 2 at.% at room temperature. Co solubility in polycrystals with grain sizes between 100 and 1000 nm is much higher than in the coarse-grained samples (Fig. 4). For example, it is two times higher at 800 °C and about four times higher at 550 °C.

Fine powders were chemically synthesized from various aqueous solutions, dried and sintered (without compaction) at temperatures between 150 and 900 °C[29,30]. TEM micrographs published in Refs. [29,30] permitted us to estimate the ratio between the GB area and the free surface area as being between 10% and 50%. Fine powders may also be produced by the ball milling of commercially available Co and Zn oxides which were compacted before sintering [31,32]. In this case the portion of GBs reaches nearly 100%. Reactive magnetron co-sputtering was used for the growth of Co-doped ZnO thin films on the Si/SiO_2 substrates using Zn and CoFe metal targets [34]. A mixed plasma of Ar and O_2 was used for sputtering, and the substrate temperature was 600 °C. The composition of the film was controlled by the sputtering ratio of each target. The films contain poreless elongated columnar grains with a grain diameter of about 100 nm. Films can also be sputtered from a single-compound ZnCoO target [35–37].

In Ref. [37] the Co-doped ZnO thin films were prepared by a sol–gel coating route using $Zn(CH_3COO)_2{\cdot}H_2O$ and $Co(CH_3COO)_2{\cdot}H_2O$ as starting precursors and a 9:1 mixture of 2-methoxyethanol and ethanolamine as a solvent. The sol–gel-coated films were finally heat-treated at 600 °C for 10 min in a reduced oxygen pressure at 1 Pa by rapid thermal annealing. The films contain grains about 100 nm in size. The sol–gel method was also used in Refs. [38–41]. The densely arranged nanowires with multiple contacts (GBs) can be grown with the aid of electrodeposition [42,43]. For example, the nanowires with diameters of 100–200 nm and about 2 mm in length were grown from the aqueous solution containing zinc nitrate hydrate and cobalt nitrate hydrate at 90 °C. A negative potential of −0.8 V relative to a gold reference electrode was applied to a silicon substrate [42]. In Ref. [33] the Co-doped ZnO was melted inside a glass balloon by using solar heating power focused on the sample by means of a curved focusing mirror, vapourized and then condensed. This vapourization–condensation method yielded a few micrometer-long wires and tetrapodes with diameters slightly above 100 nm [33]. Multiple contacts (GBs) between individual wires are present in such samples, and they are visible in TEM and scanning electron microscopy (SEM) micrographs.

In Fig. 6 the solubility limit (solvus) of Co in ZnO polycrystals is drawn using the data on polycrystals with grain size between 20 and 100 nm [29,36,37,46,48,30,49–109]. These samples were obtained by full or partial sintering of very fine powders [29,48,30,49–58], partial sintering of nanowires [59–65], autocombustion method [66], vapourization–condensation method [33], magnetron sputtering [36,37,67–76], ion beam sputtering [77], ion implantation [78–80], molecular beam epitaxy [81–83], sol–gel method [84–90], chemical vapour deposition (CVD) [91–93] and PLD [46,94–109]. The crosses correspond to the experiments where TEM investigations were performed; GBs are visible in TEM micrographs and GB Co-rich phases are absent [29,46,70,73–75,83,94–96,103]. The solubility of Co in ZnO drastically increased in comparison with Fig. 3. It reached about 25 at.% at 700 °C and remained above 12 at.% at room temperature.

Nanowires and nanorods were grown from various solutions [59–65]. For example, in Ref. [59] the nanowires were synthesized by the thermal decomposition of zinc acetate and cobalt(II) acetate in refluxing trioctylamine. During the growth and following heat treatment, single-crystalline nanowires and nanorods grow together, forming GBs. The (usually low) amount of GBs can be estimated from SEM and TEM micrographs. In the autocombustion method [66] the Zn and Co powders were mixed with fuel, where glycine (2 mole of glycine per mole of metal ion) or a mixture of glycine and dextrose (2 mole of glycine + 1 mole of dextrose) were used as fuel. The combustion of a metal–

fuel mixture made it possible to produce the fine powders of the Co-doped zinc oxide with partially sintered 20–45 nm grains. Ion beam sputtering is similar to the double-target magnetron sputtering [77]. Two targets containing Zn and Co were simultaneously or alternately sputtered by the ion beam. The layers deposited on the single-crystalline sapphire substrates were then annealed in various atmospheres at 250 °C.

Variants of CVD (PIMOCVD—pulse-injection, oxygen plasma assisted metal organic CVD, or ultrasonic-assisted CVD) are simple soft processes which permit film growth from either organic or inorganic precursors [91–93]. Deposition can be carried out in the absence of a vacuum. During the PIMOCVD process [92] small droplets of a monoglyme solvent with $Zn(tmhd)_2$ and $Co(tmhd)_3$ (tmhd = 2,2,6,6-tetramethyl-3,5-heptanedionate) were sequentially pulsed into a hot evaporation chamber. This evaporation chamber was heated to a temperature that is high enough to rapidly evaporate the injected solution but low enough to avoid precursor decomposition. An $Ar:O_2$ 1:1 carrier gas was subsequently used to transport small amounts of evaporated precursor to the deposition chamber, in which thermal decomposition and thin film growth occurred. The substrate temperature during deposition was 550 °C. After the deposition, the samples were slowly cooled to room temperature in an oxygen pressure of 1 atm and dense nanocrystalline textured films were formed [91–93].

In Fig. 7 the solubility limit (solvus) of Co in ZnO polycrystals is drawn using the data on polycrystals with grain size below 20 nm [26–28,35,49,60,62,68,71,73,74,76,85,86,91,92,97,105,110–126]. These samples were obtained by sintering very fine powders [49,110–112], solution combustion method [113], partial sintering of nanowires [60,62,97,112,114], magnetron sputtering [35,68,71,73,74,76,115–121], ion beam sputtering [122,123], sol–gel method [85,86], CVD [91,92] and PLD [26–28,105,124–126]. The data obtained in this work for samples with $d = 10$ nm (liquid ceramics method, Fig. 3) are also present at 550 °C. As in Fig. 6, crosses correspond to the experiments where TEM investigations were performed; GBs are visible in TEM micrographs and GB Co-rich phases are absent [105,117,120,123]. The solubility of Co in ZnO drastically increased in comparison with Fig. 6 where it reached about 40 at.% at 500 °C and remained above 22 at.% at room temperature.

In Fig. 8 the solubility limit (solvus) of Co in ZnO single crystals is drawn using the data on powder samples with different particle sizes [10–12,15–18,32,19,127–132]. The data are much scarcer in comparison with polycrystals (Figs. 1–4). The single crystals, particles, rods, wires, etc., without GBs were obtained by growing Co-doped ZnO single crystals from the melt [11], conventional milling [10,17–19], ball milling of micro- and nanopowders [32,54,57,111,127], mechanical alloying [56], thermal decomposition of aqueous and organic acetate solutions [128,129], chemical vapour transport [15,16], vapourization–condensation method in a solar reactor [130], direct hydrothermal synthesis [131], high-temperature and high-pressure synthesis [12] and sol–gel synthesis [132]. The solubility lines (1) for the particle size above 1000 nm, (2) between 20 and 100 nm and (3) for particles with a size of 6 nm are shown in Fig. 8. The solubility limit (solvus) for the large crystals (particles and/or grains larger than 1000 nm) is the same as in Fig. 4. It can be seen that decreasing the particle size also increases the solubility of Co in ZnO. However, in this case c_{sa} shifts to the right much weaker than in Figs. 5–7 (poreless polycrystals). This difference demonstrates that GBs in ZnO can accumulate much more Co atoms than free surfaces.

Based on the knowledge that Co solubilities depend on grain and particle size (Figs. 4–8), it is possible to estimate the maximum Co segregation in ZnO GBs and free surfaces. Let us calculate first the area to volume ratio for the grains and particles. If we suppose that grains and particles are spheres with diameter D, the surface for each particle is πD^2 and the GB area for each grain is $\pi D^2/2$ (since each GB is shared between two neighbouring grains). The volume for spherical grains and particles is the same, namely $\pi D^3/6$. Thus the area to volume ratio, A, for the free surfaces of spherical particles is $A_{FS} = 3/D$ and for GBs of spherical grains $A_{GB} = 3/2D$. One of the earliest studies of grain shape was made by Lord Kelvin [133]. He showed that the optimal space-filling grain shape, with a minimal surface area and surface tension, is a polyhedron known as a tetrakaidecahedron, which has 14 faces, 24 corners and 36 edges. A tetrakaidecahedron is an octahedron truncated by a cube. For the Kelvin tetrakaidecahedron the ratio of surface area to that of a sphere of the same volume is 1.099 [134]. Thus the area to volume ratio for grains is $A_{GB} = 1.65/D$. If one monolayer (ML) of Co covers ZnO free surfaces or GBs, their input, c_{FS} or c_{GB}, in the full concentration can be calculated as the product of A_{FS} or A_{GB} and the thickness, d, of a surface or GB layer. d can be estimated as the cube root of the unit cell volume. The unit cell volume for ZnO containing a small amount of Co is about 47×10^{-3} nm^{-3} according to our measurements. Thus $d = 0.36$ nm^{-1}. Therefore, for the one ML, $c_{FS} = dA_{FS} = 1.08/D$ and $c_{GB} = dA_{GB} = 0.59/D$.

In Fig. 9 the input of Co accumulated in GBs and surfaces in total concentration is shown for different grain size. c_{FS} and c_{GB} values for 1 ML are shown by thin and thick straight lines, respectively. On the log–log scale these lines have a slope of −0.5. The solubility limit of Co in the single-crystalline or coarse-grained ZnO at 500 and 600 °C is 2 and 2.5 at.% Co, respectively (Fig. 4). If we subtract these values from the solubility limit of Co in the fine-grained ZnO (Figs. 5–8), we obtain the input of GB, c_{GB}, or free surface segregation, c_{FS}, into total Co solubility in the ZnO polycrystals. The c_{GB} values are shown in Fig. 9 by full circles (500 °C) and full hexagons (600 °C). It is easy to see that the experimental c_{GB} values are almost one order of magnitude higher than the calculated values for 1 ML. Moreover, the slope of the lines for GB input is slightly lower than 0.5. It means that the GB input in the

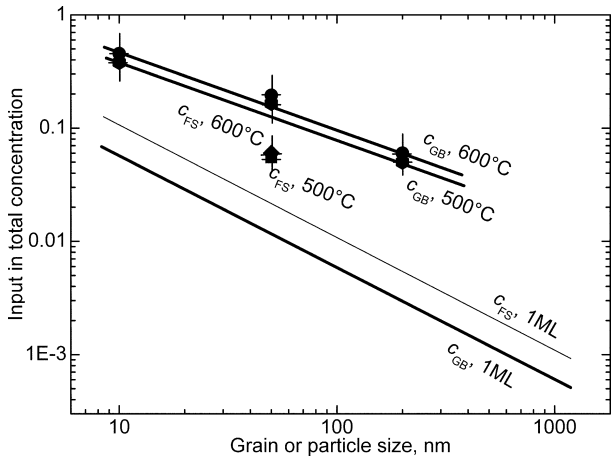

Fig. 9. Size dependence of the input of GB or surface segregation of Co into full Co content.

total Co concentration increases with decreasing grain size. The c_{FS} points for free surfaces (full square and full diamond) lie much lower than the c_{GB} values for GBs. This means that free surfaces can accumulate much less Co in comparison with GBs.

Fig. 9 undoubtedly indicates that the Co-enrichment of GBs in fine-grained ZnO cannot be reduced to the simple single-layer GB segregation analyzed by McLean [1]. First, for a given grain size, McLean-like models would predict an almost constant level of segregation with increasing temperature when following a solvus line. This is contrary to the trends shown by the data presented in Figs. 4–7, which demonstrate the drastically increasing apparent solubility with increasing temperature. Also, conventional segregation cannot predict adsorbed layers that are about 10 ML thick. Most likely, the layers of a GB phase of a finite thickness have to be considered which are not segregated layers in the conventional sense, nor are they conventional wetting films of a second phase.

Such thin GB layers of constant thickness of few nanometers were first observed and theoretically treated with the aid of force-balance models in the pioneering works of David A. Clarke on silicon nitride [135–138]. Later, nanometer-thick, disordered films of a nearly constant or "equilibrium" thickness have been frequently observed in GBs in ceramics [136–148] and oxide/metal interfaces [149–153]. According to the force-balance models, such finite thickness wetting films would only occur when there are attractive interactions between the two interfaces that confine the wetting film; it is again neither a conventional segregation nor a conventional wetting situation. Cannon and Esposito further argued that the Clarke model is actually a high-temperature colloidal theory [147]. The intergranular films can alternatively be understood to be multilayer adsorbates at GBs [154]. The GB films of equilibrium thickness can be observed by TEM (or by high-resolution electron microscopy, HREM), but in any case they remain invisible to conventional XRD and, therefore, affect the increase in the apparent solubility with decreasing grain size.

Thin equilibrium GB or surface films in the single-phase area of a bulk phase diagram were first considered by Cahn [147]. He proposed the idea that the transition from incomplete to complete surface wetting is a phase transformation. Later this idea was successfully applied to GBs, and old data on GB wetting were also reconsidered from this point of view [154–157]. GB wetting phase transformation proceeds at the temperature T_{wGB} where GB energy σ_{GB} becomes equal to the energy $2\sigma_{SL}$ of two solid–liquid interfaces. Above T_{wGB} GB is substituted by a layer of the melt. The tie-line of the GB wetting phase transition in the two-phase area of a bulk phase diagram continues into the one-phase area as a prewetting (or GB solidus) line. In the area between GB solidus and bulk solidus, GB contains the thin layer of a GB phase. The energy gain $(\sigma_{GB} - 2\sigma_{SL})$ above T_{wGB} permits stabilization of such a thin layer of a GB phase between the abutting crystals, which is metastable in the bulk and becomes stable in the GB. The formation of metastable phase layer of thickness l leads to the energy loss $l\Delta g$. The finite thickness l of the GB phase is defined by the equality of the energy gain $(\sigma_{GB} - 2\sigma_{SL})$ and energy loss $l\Delta g$. In this simplest model, the prewetting GB layer of finite thickness l suddenly appears by crossing the prewetting (GB soludus) line $c_{bt}(T)$. Thickness l logarithmically diverges close to the bulk solidus. This is due to the fact that the thickness of a wetting phase is thermodynamically infinite in the two-phase area. Physically, in the two-phase area, its thickness is defined only by the amount of the wetting phase. Several ML thick liquid-like GB layers possessing high diffusivity were observed in the Cu–Bi [158–162], Al–Zn [163–165], Fe–Si–Zn [166–171] and W–Ni alloys [172,173]. The direct HREM evidence for thin GB films and triple junction "pockets" has been recently obtained in metallic W–Ni [172,173] and Al–Zn [164] alloys. GBs can also be "wetted" by a second solid phase, and the reversible transition from incomplete to complete solid phase wetting was observed for the first time in the Zn–Al system at a certain temperature T_{ws} [160]. Cahn's ideas remain valid also in this case, and the GB solvus line should exist in the single-phase area of the bulk phase diagram, which starts at the point where the GB wetting tie-line intersects.

Later, Cahn's critical point wetting model was developed further and generalized [174–176]. In the simplest approach, a sequence of three regions, namely submonolayer/monolayer adsorption, nanoscale interfacial films/multilayer adsorption, and finely complete wetting, can occur in the bulk phase diagram with increasing concentration (activity) of a second component (dopant) [177]. Additional complexity comes from the possible occurrence of GB roughening [163], GB layering [177], pseudo-partial (or frustrated-complete) melting/wetting [178], first-order or continuous adsorption/wetting transitions [187] and interfacial critical points [167,168]. It cannot be excluded that in the nanograined ZnO–CoO polycrystals the situation is more complicated than the simple sequence monolayer adsorption → interfacial film → macroscopically thick complete wetting film. Therefore, the ZnO–CoO sys-

tem demands more detailed investigation. It cannot be excluded that the GB films and triple junction "pockets" would be technologically applicable as those in the ZnO–Bi_2O_3 polycrystals (used in varistors since the 1970s) [139,140,178–186]. Another approach to the explanation of GB films (or so-called GB complexions) was developed by Harper and coworkers for Al_2O_3-based ceramics [188,189].

The additional increase in the GB input in the total Co concentration with decreasing grain size (Fig. 9) may also be an indication of the increasing input of GB triple joints. It has been observed in the Al–Zn system that the triangle of "pockets" of a prewetting phase in the GB triple joints are thicker than the prewetting GB layers [166,167]. A similar conclusion can also be drawn from the analysis of TEM micrographs of some nanometer-thick GB layers and triple joint "pockets" of amorphous phase in ceramics [136–148,178–186].

The logarithmic divergence of the GB layer thickness predicted by the Cahn model may be the reason for the high value of GB thickness obtained from Fig. 9. The lines in Fig. 9 were calculated based on the apparent shift in the solubility. Therefore, the resulting GB thickness corresponds to that at the solubility (solvus) line. Several consequences, which will be experimentally tested by us in the future, follow from this result. First, thin layers of a Co-rich GB phase are present in the micro- and nanograined ZnO close to the solvus line. Second, the Co-rich bulk oxide must wet the ZnO GBs in the two-phase area of the bulk phase diagram above a certain temperature, T_{ws}. Third, it is evident that at very low Co concentrations, GBs in ZnO contain the conventional McLean-like segregation layers. Therefore, one can expect to observe a jump-like transition from the conventional segregation to the GB layer of finite thickness at a certain bulk concentration, c_{bt}, between 0 at.% Co and c_s. This is just the simplest expectation; in reality the situation could be much more complex [177].

One can estimate the lower limit for c_{bt} using the structural data obtained by TEM in the papers we used to construct the diagram in Figs. 3–7. The experimental works where the GB structure is visible in TEM micrographs are marked by crosses in Figs. 6 and 7 [29,46,70,73–75,83,94–96,103,105,117,120,123]. No Co-rich GB layers or phases were observed in these cases. It can be seen that in all cases the Co concentration was rather low and far away from solubility limit. Dashed lines in Figs. 6 and 7 denote the hypothetical position of GB solvus $c_{bt}(T)$ separating the area without Co-rich GB phases (TEM observations) from the area where the Co-rich GB phase can exist (estimations in Fig. 9).

The nanometer-thick GB films of a nearly constant or "equilibrium" thickness have been widely observed in ZnO doped with Bi_2O_3 [139,140,178–186]. ZnO doped with Bi is used in the manufacturing of varistors. Varistors exhibit highly nonlinear current–voltage characteristics with a high resistivity below a threshold electric field, becoming conductive when this field is exceeded. This phenomenon enables them to be used in current oversurge protection circuits [190]. After liquid-phase sintering, such material consists of ZnO grains separated by thin Bi_2O_3-rich GB layers. Interfaces between ZnO grains control the nonlinear current–voltage characteristics. The presence of a few nanometer-thick Bi-rich GB phases in ZnO is governed by the GB wetting phase transformation. It is interesting that along with the simplest Cahn model of the transition from partially wetted GBs to completely wetted ones, a more complicated situation was also observed in the ZnO–Bi_2O_3 system, namely the transition from pseudo-partially wetted GBs to the completely wetted ones [178]. In this case a thin GB layer may exist in the equilibrium with thick Bi_2O_3 droplets having nonzero contact angle in the GB plane. The most recent study demonstrated that the real situation is even more complicated: the transition from pseudo-partially wetted GBs to the completely wetted GBs is in fact inhibited by an attractive van der Waals dispersion force in the ZnO–Bi_2O_3 system [191]. The extensive number of published structural investigations [139,140,178–186] allowed us to construct the GB lines in the ZnO–Bi_2O_3 bulk phase diagram [190] which corresponds with the diagram published in Ref. [192].

A few nanometer-thick Bi-rich layers were observed also in the ZnO surfaces [192,193,178,194]. Their thickness was close to that of GB layers [178]. The thickness of surface films was explained by the incomplete-partial (frustrated-complete) surface wetting [194]. In case of the frustrated-complete wetting, the thickness of a surficial (or GB) film also increases with increasing dopant concentration (activity) and can reach a few MLs. However, it does not diverge by approaching the solubility limit line like GB (or surface) films in the case of complete wetting and remains finite [177,191,192]. In the case of Co-doped ZnO, the estimation presented in Fig. 9 predicts lower Co capacity of free surfaces in comparison with GBs. This fact has to be carefully investigated in future experiments. It may be an indication of complete wetting in GBs and frustrated-complete wetting in surfaces. Recent observation of thin GB layers of the Fe-rich phase in Fe-doped nanograined ZnO also increases the chances of success in searching for Co-enriched GB layers in ZnO [195]. Therefore, based on the results obtained in this work one can expect to observe in the future various interesting GB phases and phase transformations in Co-doped ZnO. Furthermore, the observed shift of the solvus line in the Co-doped ZnO will also explain the mysterious phenomenon of room-temperature ferromagnetism in the broad-band transparent semiconductor ZnO.

4. Conclusions

1. The accumulation of Co in GBs and free surfaces drastically shifts the Co solubility limit in ZnO to higher Co concentrations. For example, at 550 °C the total solubility in the bulk is below 2 at.% Co. However, it is about 40 at.% Co in the nanograined sample with a grain size below 20 nm.

2. A small grain size leads to a larger solubility shift when compared with similarly small particle sizes. This means that the Co accumulation ability of GBs is about 2–4 times higher than that of free surfaces.
3. Thus, the phase diagrams for the materials having a grain size below 1000 nm have to be reinvestigated. An especially drastic change in the phase diagrams can be expected when the grain size is below 100 nm.

Acknowledgements

Authors thank the Russian Foundation for Basic Research (projects 08-08-90105 and 08-08-91302), Deutsche akademische Austauschdienst (DAAD), Deutsche Forschungsgemeinschaft (DFG) and the German Federal Ministry for Education and Science (BMBF) for the financial support of investigations and exchange travel. Authors cordially thank Prof. G. Schütz, Dr. D. Goll and Dr. E. Goering for stimulating discussions, Dr. A. Nekrasov for the help with EPMA measurements, Ms. J. Breithaupt for improving the English.

References

[1] McLean D. Grain boundaries in metals. Oxford: Clarendon Press; 1957. p. 120.
[2] Trudeau ML, Huot JY, Schulz R. Appl Phys Lett 1991;58:2764.
[3] Suzuki K, Makino A, Inoue A, Masumoto T. J Appl Phys 1991;70:6232.
[4] Heera V, Madhusoodanan KN, Skorupa W, Dubois C, Romanus H. J Appl Phys 2006;99:123716.
[5] Kim M, Laine RM. J Ceram Proc Res 2007;8:129.
[6] Lemier C, Weissmüller J. Acta Mater 2007;55:1241.
[7] Rizea A, Chirlesan D, Petot C, Petot-Ervas G. Solid State Ionics 2002;146:341.
[8] Dietl T, Ohno H, Matsukura F, Cibert J, Ferrand D. Science 2000;287:1019.
[9] Soyer A. J Appl Crystallogr 1995;28:244.
[10] Bates CH, White WB, Roy R. J Inorg Nucl Chem 1966;28:397.
[11] Kane MH, Fenwick WE, Strassburg M, Nemeth B, Varatharajan R, Song Q, et al. Phys Status Solidi B 2007;244:1462.
[12] Yin S, Xu MX, Yang L, Liu JF, Rösner H, Hahn H, et al. Phys Rev B 2006;73:224408.
[13] Zhang Z, Chen Q, Lee HD, Xue YY, Sun YY, Chen H, et al. J Appl Phys 2006;100:043909.
[14] Borges RP, Pinto JV, da Silva RC, Gonçalves AP, Cruz MM, Godinho M. J Magn Magn Mater 2007;316:E191.
[15] Szuszkiewicz W, Morhange JF, Golacki Z, Lusakowski A, Schumm M, Geurts J. Acta Phys Pol A 2007;112:363.
[16] Millot M, Gonzalez J, Molina I, Salas B, Golacki Z, Broto JM, et al. J Alloys Compd 2006;423:224.
[17] Wen QY, Zhang HW, Song YQ, Yang QH, Xiao JQ. Chin Phys Lett 2007;24:2955.
[18] Nipan GD, Ketsko VA, Kol'tsova TN, Stognii AI, Yanushkevich KI, Pan'kov VV, et al. Russ J Inorgan Chem 2006;51:1961.
[19] Kolesnik S, Dabrowski B, Mais J. J Appl Phys 2004;95:2582.
[20] Wi SC, Kang JS, Kim JH, Lee SS, Cho S-B, Kim BJ, et al. Phys Status Solidi B 2004;241:1529.
[21] Wang YQ, Yuan SL, Song YX, Liu L, Tian ZM, Li P, et al. Chin Sci Bull 2007;52:1019.
[22] Okamoto M, Inoue Y, Kawahara T, Morimoto Y. Jpn J Appl Phys Part 1 2005;44:4461.
[23] Zhang YB, Sritharan T, Li S. Phys Rev B 2006;73:172404.
[24] Zhu T, Zhan WS, Wang WG, Xiao JQ. Appl Phys Lett 2006;89:022508.
[25] Bouloudenine M, Viart N, Colis S, Kortus J, Dinia A. Appl Phys Lett 2005;87:052501.
[26] Peng YZ, Liew T, Chong TC, Song WD, Li HL, Liu W. J Appl Phys 2005;98:114909.
[27] Peng YZ, Liew T, Chong TC, An CW, Song WD. Appl Phys Lett 2006;88:192110.
[28] Peng YZ, Song WD, An CW, Qiu JJ, Chong JF, Lim BC, et al. Appl Phys A 2005;80:565.
[29] Hays J, Thurber A, Reddy KM, Punnoose A, Engelhard MH. J Appl Phys 2006;99:08M123.
[30] Chang GS, Kurmaev EZ, Boukhvalov DW, Finkelstein LD, Colis S, Pedersen TM, et al. Phys Rev B 2007;75:195215.
[31] Wang Y, Sun L, Kong LG, Kang J-F, Zhang X, Han R-Q. J Alloys Compd 2006;423:256.
[32] Quesada A, Garcia MA, Andres M, Hernando A, Fernández JF, Caballero AC, et al. J Appl Phys 2006;100:113909.
[33] Martinez B, Sandiumenge F, Balcells L, Fontcuberta J, Sibieude F, Monty C. J Magn Magn Mater 2005;290:168.
[34] Cho YM, Choo WK, Kim H, Kim D, Ihm TE. Appl Phys Lett 2002;80:3358.
[35] Yan SS, Ren C, Wang X, Xin Y, Zhou ZX, Mei LM, et al. Appl Phys Lett 2004;84:2376.
[36] Lee HJ, Park CH, Jeong SY, Yee K-J, Cho CR, Jung MH, et al. Appl Phys Lett 2006;88:062504.
[37] Park JH, Kim MG, Jang HM, Ryu S, Kim YM. Appl Phys Lett 2004;84:1338.
[38] Lee HJ, Ryu GH, Kim SK, Kim SA, Lee C-H, Jeong S-Y, et al. Phys Status Solidi B 2004;241:2858.
[39] Zhou HJ, Chen LM, Malik V, Knies C, Hofmann DM, Bhatti KP, et al. Phys Status Solidi A 2007;204:112.
[40] Shi TF, Zhu SY, Sun ZH, Wei S, Liu W. Appl Phys Lett 2007;90:102108.
[41] Liu XC, Shi EW, Chen ZZ, Zhang H-W, Zhang T, Song L-X. Chin Phys 2007;16:1770.
[42] Cuiand JB, Gibson UJ. Appl Phys Lett 2005;87:133108.
[43] Cui JB, Zeng Q, Gibson UJ. J Appl Phys 2006;99:08M113.
[44] Peng YZ, Thomas L, Ye ZZ, Zhang YZ. Chin Sci Bull 2007;52:2742.
[45] Stamenov P, Venkatesan M, Dorneles LS, Maude D, Coey JMD. J Appl Phys 2006;99:08M124.
[46] Gacic M, Jakob G, Herbort C, Adrian H, Tietze T, Brück S, et al. Phys Rev B 2007;75:205206.
[47] Samanta K, Bhattacharya P, Katiyar RS, Iwamoto W, Pagliuso PG, Rettori C. Phys Rev B 2006;73:245213.
[48] Wang XF, Xu JB, Zhang B, Yu H, Wang J, Zhang X, et al. Adv Mater 2006;18:2476.
[49] Ghosh CK, Chattopadhyay KK, Mitra MK. J Appl Phys 2007;101:124911.
[50] Wang XF, Xu JB, Ke N, Yu J, Wang J, Li Q, et al. Appl Phys Lett 2006;88:223108.
[51] Maensiri S, Laokul P, Phokha S. J Magn Magn Mater 2006;305:381.
[52] Rubi D, Calleja A, Arbiol J, Capdevila XG, Segarra M, Aragones L, et al. J Magn Magn Mater 2007;316:e211.
[53] Liu WK, Salley GM, Gamelin DR. J Phys Chem B 2005;109:14486.
[54] Bouloudenine M, Viart N, Colis S, Dinia A. Catal Today 2006;113:240.
[55] Jayakumar OD, Gopalakrishnan IK, Kulshreshtha SK. Adv Mater 2006;18:1857.
[56] Damonte LC, Hernández-Fenollosa MA, Meyer M, Mendoza-Zélis L, Marí B. Phys B 2007;398:380.
[57] Colis S, Bieber H, Bégin-Colin S, Schmerber G, Leuvrey C, Dinia A. Chem Phys Lett 2006;422:529.
[58] Quesada A, Garcia MA, Andrés M, Hernando A, Fernández JF, Caballero AC, et al. J Appl Phys 2006;100:113909.
[59] Yuhas BD, Zitoun DO, Pauzauskie PJ, He R, Yang P. Angew Chem Int Ed 2006;45:420.

[60] Bi H, Chen QW, You FY, Zhou XL. Chin Phys Lett 2006;23:1907.
[61] Wang H, Wang HB, Yang FJ, Chen Y, Zhang C, Yang CP, et al. Nanotechnology 2006;17:4312.
[62] Chu DW, Zeng YP, Jiang DL. J Am Ceram Soc 2007;90:2269.
[63] Clavel G, Pinna N, Zitoun D. Phys Status Solidi A 2007;204:118.
[64] Chiou JW, Tsai HM, Pao CW, Krishna Kumar KP, Ray SC, Chien FZ, et al. Appl Phys Lett 2006;89:043121.
[65] Jian WB, Wu ZY, Huang RT, Chen FR, Kai JJ, Wu CY, et al. Phys Rev B 2006;73:233308.
[66] Deka S, Pasricha R, Joy PA. Phys Rev B 2006;74:033201.
[67] Dinia A, Schmerber G, Mény C, Pierron-Bohnes V, Beaurepaire E. J Appl Phys 2005;97:123908.
[68] Lim SW, Hwang DK, Myoung JM. Solid State Commun 2003;125:231.
[69] Huang B, Zhu DL, Ma XC. Appl Surf Sci 2007;253:6892.
[70] Song C, Zeng F, Geng KW, Pan F, He B, Yan WS. Phys Rev B 2007;76:045215.
[71] Tay M, Wu YH, Han GC, Chong TC, Zheng YK, Wang SJ, et al. J Appl Phys 2006;100:063910.
[72] Choi CH, Kim SH. Thin Solid Films 2007;515:2864.
[73] Liu XJ, Song C, Zeng F, Wang XB, Pan F. J Phys D 2007;40:1608.
[74] Zhao ZW, Tay BK, Chen JS, Hu JF, Lim BC, Li GP. Appl Phys Lett 2007;90:152502.
[75] Song C, Zeng F, Geng KW, Wang XB, Shen YX, Pan F. J Magn Magn Mater 2007;309:25.
[76] Liu XC, Shi EW, Chen ZZ, Zhang H-W, Songa L-X, Wang H, et al. J Cryst Growth 2006;296:135.
[77] Hsu HS, Huang JCA, Huang YH, Liao YF, Lin MZ, Lee CH, et al. Appl Phys Lett 2006;88:242507.
[78] Wu ZY, Chen FR, Kai JJ, Jian WB, Lin JJ. Nanotechnology 2006;17:5511.
[79] Kumar R, Singh F, Angadi B, Choi J-W, Choi W-K, Jeong K, et al. J Appl Phys 2006;100:113708.
[80] Angadi B, Jung YS, Choi WK, Kumar R, Jeong K, Shin SW, et al. Appl Phys Lett 2006;88:142502.
[81] Liu GL, Cao Q, Deng JX, Xing PF, Tian YF, Chen YX, et al. Appl Phys Lett 2007;90:052504.
[82] Lee HJ, Lee SH, Yildiz F, Jeong YH. J Magn Magn Mater 2007;310:2089.
[83] Nielsen K, Bauer S, Luebbe M, Goennenwein STB, Opel M, Simon J, et al. Phys Status Solidi A 2006;203:3581.
[84] Lee HJ, Jeong SY, Cho CR, Park CH. Appl Phys Lett 2002;81:4020.
[85] Hays J, Reddy KM, Graces NY, Engelhard MH, Shutthanandan V, Luo M, et al. J Phys Condens Matter 2007;19:266203.
[86] Glaspell G, Dutta P, Manivannan A. J Cluster Sci 2005;16:523.
[87] Belghazi Y, Schmerber G, Colis S, Rehspringer JL, Berrada A, Dinia A. J Magn Magn Mater 2007;310:2092.
[88] Belghazi Y, Schmerber G, Colis S, Rehspringer JL, Dinia A, Berrada A. Appl Phys Lett 2006;89:122504.
[89] Manivannan A, Dutta P, Glaspell G, Seehraa MS. J Appl Phys 2006;99:08M110.
[90] Zhou HJ, Knies C, Hofmann DM, Stehr J, Volbers N, Meyer BK, et al. Phys Status Solidi A 2006;203:2756.
[91] Khare N, Kappers MJ, Wei M, Blamire MG, MacManus-Driscoll JL. Adv Mater 2006;18:1449.
[92] Zukova A, Teiserskis A, van Dijken S, Gun'ko YK, Kazlauskiene V. Appl Phys Lett 2006;89:232503.
[93] Chambers SA, Schwartz DA, Liu WK, Kittilstved KR, Gamelin DR. Appl Phys A 2007;88:1.
[94] Ramachandran S, Tiwari A, Narayan J. J Electron Mater 2004;33:1298.
[95] Prater JT, Ramachandran S, Tiwari A, Narayan J. J Electron Mater 2006;35:852.
[96] Chakraborti D, Ramachandran S, Trichy G, Narayan J, Prater JT. J Appl Phys 2007;101:053918.
[97] Xu QY, Hartmann L, Schmidt H, Hochmuth H, Lorenz M, Schmidt-Grund R, et al. Phys Rev B 2006;73:205342.
[98] Xu QY, Hartmann L, Schmidt H, Hochmuth H, Lorenz M, Schmidt-Grund R, et al. J Appl Phys 2006;100:013904.
[99] Xu QY, Hartmann L, Schmidt H, Hochmuth H, Lorenz M, Schmidt-Grund R, et al. Thin Solid Films 2006;515:2549.
[100] Schmidt H, Diaconu M, Hochmuth H, Benndorf G, von Wenckstern H, Biehne G, et al. Appl Phys A 2007;88:157.
[101] Prellier W, Fouchet A, Simon C, Mercey B. Mater Sci Eng B 2004;109:192.
[102] Dorneles LS, O'Mahony D, Fitzgerald CB, McGee F, Venkatesan M, Stanca I, et al. Appl Surf Sci 2005;248:406.
[103] Zhang YB, Liu Q, Sritharan T, Gan CL, Li S. Appl Phys Lett 2006;89:042510.
[104] Kobayashi M, Ishida Y, Hwang JI, Mizokawa T, Fujimori A, Mamiya K, et al. Phys Rev B 2005;72:201201.
[105] Liu Q, Yuan CL, Gan CL, Han GC. J Appl Phys 2007;101:073902.
[106] Neal JR, Behan AJ, Ibrahim RM, Blythe HJ, Ziese M, Fox AM, et al. Phys Rev Lett 2006;96:197208.
[107] Xu XH, Blythe HJ, Ziese M, Behan AJ, Neal JR, Mokhtari A, et al. New J Phys 2006;8:135.
[108] Saeki H, Matsui H, Kawai T, Tabata H. J Phys Condens Matter 2004;16:S5533.
[109] Budhani C, Pant P, Rakshit RK, Senapati K, Mandal S, Pandey NK, et al. J Phys Condens Matter 2005;17:75.
[110] Mandal SK, Das AK, Nath TK, Karmakar D, Satpati B. J Appl Phys 2006;100:104315.
[111] Volbers N, Zhou H, Knies C, Pfisterer D, Sann J, Hofmann DM, et al. Appl Phys A 2007;88:153.
[112] Qiu XQ, Li LP, Tang CL, Li G. J Am Chem Soc 2007;129:11908.
[113] Deka S, Joy PA. Appl Phys Lett 2006;89:032508.
[114] Qiu XQ, Li LO, Li GS. Appl Phys Lett 2006;88:114103.
[115] Yin Z, Chen N, Chai C, Yang F. J Appl Phys 2004;96:5093.
[116] Dinia A, Ayoub JP, Schmerber G, Beaurepaire E, Muller D, Grobb JJ. Phys Lett 2004;333:152.
[117] Song C, Geng KW, Zeng F, Wang XB, Shen YX, Pan F, et al. Phys Rev B 2006;73:024405.
[118] Song C, Pan SN, Liu XJ, Li XW, Zeng F, Yan WS, et al. J Phys Condens Matter 2007;19:176229.
[119] Kim YS, Ko YD, Tai WP. J Electroceram 2006;17:235.
[120] Song C, Liu XJ, Geng KW, Zeng F, Pan F, He B, et al. J Appl Phys 2007;101:103903.
[121] Antony J, Pendyala S, Sharma A, Chen XB, Morrison J, Bergman L, et al. J Appl Phys 2005;97:10D307.
[122] Pakhomov AB, Roberts BK, Tuan A, Shutthanandan V, McCready D, Thevuthasan S, et al. J Appl Phys 2004;95:7393.
[123] Hsu HS, Huang JCA, Chen SF, Liu CP. Appl Phys Lett 2007;90:102506.
[124] Liu YZ, Xu QY, Schmidt H, Hartmann L, Hochmuth H, Lorenz M, et al. Appl Phys Lett 2007;90:154101.
[125] Ueda K, Tabata H, Kawai T. Appl Phys Lett 2001;79:988.
[126] Martinez-Criado G, Segura A, Sans JA, Homs A, Pellicer-Porres J, Susini J. Appl Phys Lett 2006;89:061906.
[127] Bartolome F, Blasco J, García LM, García J, Jiménez S, Lozano A. J Magn Magn Mater 2007;316:E195.
[128] Kshirsagar SD, Inamdar D, Gopalakrishnan IK, Kulshreshtha SK, Mahamuni S. Solid State Commun 2007;143:457.
[129] Naeem M, Hasanain SK, Kobayashi M, Ishida Y, Fujimori A, Buzby S, et al. Nanotechnology 2006;17:2675.
[130] Martinez B, Sandiumenge F, Balcells L, Arbiol J, Sibieude F, Monty C. Phys Rev B 2005;72:165202.
[131] Yang LW, Wu XL, Qiu T, Siu GG, Chu PK. J Appl Phys 2006;99:074303.
[132] Thota S, Dutta T, Kumar J. J Phys Condens Matter 2006;18:2473.
[133] Lord Kelvin WT. Philos Mag 1887;24:503.
[134] Hosford WF. Materials science: an intermediate text. Cambridge: Cambridge University Press; 2007. p. 7.
[135] Clarke DR. J Am Ceram Soc 1987;70:15.

[136] Clarke DR, Shaw TM, Philipse AP, Horn RG. J Am Ceram Soc 1993;76:1201.
[137] Tanaka I, Kleebe H-J, Cinibulk MK, Bruley J, Clarke DR, Rühle M. J Am Ceram Soc 1994;77:911.
[138] Bobeth M, Clarke DR, Pompe W. J Am Ceram Soc 1999;82:1537.
[139] Lee J-R, Chiang Y-M, Ceder G. Acta Mater 1997;45:1247.
[140] Wang H, Chiang Y-M. J Am Ceram Soc 1998;81:89.
[141] Kleebe H-J, Hoffman MJ, Rühle M. Z Metallkd 1992;83:610.
[142] Kleebe H-J, Cinibulk MK, Cannon RM, Rühle M. J Am Ceram Soc 1993;76:1969.
[143] Chiang Y-M, Silverman LA, French RH, Cannon RM. J Am Ceram Soc 1994;77:143.
[144] Ackler HD, Chiang Y-M. J Am Ceram Soc 1997;80:1893.
[145] Chiang Y-M, Wang H, Lee J-R. J Microsc 1998;191:275.
[146] Ackler HD, Chiang Y-M. J Am Ceram Soc 1999;82:183.
[147] Cannon RM, Esposito L. Z Metallkd 1999;90:1002.
[148] Luo J, Wang H, Chiang Y-M. J Am Ceram Soc 1999;82:916.
[149] Avishai A, Scheu C, Kaplan WD. Acta Mater 2005;53:1559.
[150] Avishai A, Kaplan WD. Acta Mater 2005;53:1571.
[151] Oh SH, Kauffmann Y, Scheu C, Kaplan WD, Ruhle M. Science 2005;310:661.
[152] Levi G, Kaplan WD. J Mater Sci 2006;41:817.
[153] Baram M, Kaplan WD. J Mater Sci 2006;44:7775.
[154] Cannon RM, Rühle M, Hoffmann MJ, French RH, Gu H, Tomsia AP, et al. In: Sakuma T, Ikuhara Y, editors. Grain boundary engineering in ceramics, vol. 118. Westerville, OH: American Ceramic Society; 2000. p. 427.
[155] Cahn JW. J Chem Phys 1977;66:3667.
[156] Eustathopoulos N. Int Mater Rev 1983;28:189.
[157] Straumal B, Muschik T, Gust W, Predel B. Acta Metall Mater 1992;40:939.
[158] Straumal B, Molodov D, Gust W. J Phase Equilib 1994;15:386.
[159] Straumal BB. Grain boundary phase transitions. Moscow: Nauka; 2003. p. 327 [in Russian].
[160] López GA, Mittemeijer EJ, Straumal BB. Acta Mater 2004;52:4537.
[161] Divinski SV, Lohmann M, Herzig Chr, Straumal B, Baretzky B, Gust W. Phys Rev B 2005;71:104104.
[162] Chang L-S, Rabkin E, Straumal BB, Baretzky B, Gust W. Acta Mater 1999;47:4041.
[163] Straumal BB, Polyakov SA, Chang L-S, Mittemeijer EJ. Int J Mater Res 2007;98:451.
[164] Straumal B, Prokofjev SI, Chang L-S, Sluchanko NE, Baretzky B, Gust W, et al. Defect Diffus Forum 2001;194–199:1343.
[165] Straumal BB, Baretzky B, Mazilkin AA, Phillipp F, Kogtenkova OA, Volkov MN, et al. Acta Mater 2004;52:4469.
[166] Straumal BB, Mazilkin AA, Kogtenkova OA, Protasova SG, Baretzky B. Philos Mag Lett 2007;87:423.
[167] Straumal BB, Kogtenkova O, Zięba P. Acta Mater 2008;56:925.
[168] Rabkin EI, Semenov VN, Shvindlerman LS, Straumal BB. Acta Metall Mater 1991;39:627.
[169] Noskovich OI, Rabkin EI, Semenov VN, Straumal BB, Shvindlerman LS. Acta Metall Mater 1991;39:3091.
[170] Straumal BB, Noskovich OI, Semenov VN, Shvindlerman LS, Gust W, Predel B. Acta Metall Mater 1992;40:795.
[171] Straumal B, Rabkin E, Lojkowski W, Gust W, Shvindlerman LS. Acta Mater 1997;45:1931.
[172] Gupta VK, Yoon DH, Meyer III HM, Luo J. Acta Mater 2007;55:3131.
[173] Luo J, Gupta VK, Yoon DH, Meyer HM. Appl Phys Lett 2005;87:231902.
[174] Tang M, Carter WC, Cannon RM. Phys Rev Lett 2006;97:075502.
[175] Tang M, Carter WC, Cannon RM. Phys Rev B 2006;73:024102.
[176] Luo J, Tang M, Cannon RM, Carter WC, Chiang Y-M. Mater Sci Eng A 2006;422:19.
[177] Luo J. Crit Rev Solid State Mater Sci 2007;32:67–101.
[178] Luo J, Chiang Y-M, Cannon RM. Langmuir 2005;21:7358.
[179] Wong J. J Am Ceram Soc 1974;57:357.
[180] Wong J, Morris WG. Am Ceram Soc Bull 1974;53:816.
[181] Greuter F. Solid State Ionics 1995;75:67.
[182] Gambino JP, Kingery WD, Pike GE, Philipp HR. J Am Ceram Soc 1989;72:642.
[183] Kingery WD, van der Sande JB, Mitamura T. J Am Ceram Soc 1979;62:221.
[184] Olsson E, Falk LKL, Dunlop GL. J Mater Sci 1985;20:4091.
[185] Olsson E, Dunlop GL. J Appl Phys 1989;66:3666.
[186] Matsuoka M. Jpn J Appl Phys 1971;10:736.
[187] Straumal BB, Gornakova AS, Kogtenkova OA, Protasova SG, Sursaeva VG, Baretzky B. Phys Rev B 2008;78:032829.
[188] Dillon SJ, Harmer MP. Acta Mater 2007;55:5247.
[189] Dillon SJ, Tang M, Carter WC, Harmer MP. Acta Mater 2007;55:6208.
[190] Straumal BB, Mazilkin AA, Straumal PB, Myatiev AA. Int J Nanomanuf 2008;2:253.
[191] Qian H, Luo J, Chiang Y-M. Acta Mater 2008;56:862.
[192] Luo J, Chiang Y-M. Annu Rev Mater Res 2008;38:227.
[193] Luo J, Chiang Y-M. Acta Mater 2000;48:4501.
[194] Qian H, Luo J. Appl Phys Lett 2007;91:061909.
[195] Izaki M. Electrochemical preparation of transparent ferromagnetic Fe–Zn–O heterogranular films. In: N. Perov et al., editors. Moscow International Symposium on Magnetism. Moscow: Lomonosov State University; 2008. p. 703.